

Article

Pyrene-Modified Cyclic Peptides Detect Cu^{2+} Ions by Fluorescence in Water

Yuhi Maekawa¹, Sora Sakura¹, Yuji Furutani², Rento Fujihara¹, Hisashi Sugime^{1,*} , Takashi Ohtsuki^{2,*}  and Mizuki Kitamatsu^{1,*} 

¹ Department of Applied Chemistry, Faculty of Science and Engineering, Kindai University, 3-4-1 Kowakae, Higashi-Osaka 577-8502, Osaka, Japan

² Department of Interdisciplinary Science and Engineering in Health Systems, Okayama University, 3-1-1 Tsushimanaka, Okayama 700-8530, Okayama, Japan

* Correspondence: sugime@apch.kindai.ac.jp (H.S.); ohtsuk@okayama-u.ac.jp (T.O.); kitamatu@apch.kindai.ac.jp (M.K.)

Abstract: The detection of metal ions is an option for maintaining water quality and diagnosing metal ion-related diseases. In this study, we successfully detected metal ions using fluorescent peptides in water. First, we prepared seven linear (L1–L7) and seven cyclic (C1–C7) peptides containing two pyrenyl (Pyr) units and assessed the response to various metal ions by fluorescence. The results indicated that C1, which contains a hexameric cyclic peptide moiety consisting of Pyr and Gly units, did not show a fluorescent response to metal ions, while the linear L1 corresponding to C1 showed a response to Cu^{2+} , but its selectivity was found to be poor through a competition assay for each metal ion. We then assessed C2–C7 and L2–L7, in which Gly was replaced by His units at various positions in the same manner. The results showed that C2–C7 responded to Cu^{2+} in a manner dependent on the His position. Additionally, superior selectivity was observed in C7 through a competition assay. These results demonstrate that the structural restriction of peptides and the sequence affect the selective detection of Cu^{2+} and reveal that peptides with an appropriate structure can accomplish the fluorescent detection of Cu^{2+} specifically.

Keywords: peptide; pyrene; metal ion; fluorescence



Citation: Maekawa, Y.; Sakura, S.; Furutani, Y.; Fujihara, R.; Sugime, H.; Ohtsuki, T.; Kitamatsu, M.

Pyrene-Modified Cyclic Peptides Detect Cu^{2+} Ions by Fluorescence in Water. *Processes* **2024**, *12*, 746. <https://doi.org/10.3390/pr12040746>

Academic Editors: Kenji Usui and Kin-ya Tomizaki

Received: 11 March 2024

Revised: 1 April 2024

Accepted: 5 April 2024

Published: 7 April 2024



Copyright: © 2024 by the authors. Licensee MDPI, Basel, Switzerland. This article is an open access article distributed under the terms and conditions of the Creative Commons Attribution (CC BY) license (<https://creativecommons.org/licenses/by/4.0/>).

1. Introduction

In molecular recognition targeting ions, conventional small organic synthetic molecules show high molecular recognition in organic solvents but often do not function effectively in water because the interactions between them are canceled out by water molecules. For example, crown ethers selectively bind to specific alkali metal ions in organic solvents in a manner dependent on their ring size, but their binding affinities are very low in water [1].

Among the synthetic molecules that detect ions, the development of fluorescent probes that detect metal ions in aqueous solutions is expected to obtain probes that are easy to handle and have good sensitivity. Such probes should be useful for protecting the natural environment and diagnosing diseases related to metal ions [2]. Of these probes, those based on peptide backbones are expected to have high sequence-dependent selectivity and water solubility and have been reported by several research groups.

For example, Wu et al. reported that a tetrameric peptide, His-Gly-Gly-Gly, modified with fluorescein (Fam), selectively detected Cu^{2+} by fluorescence quenching through 1:1 binding ($K_d = 3.7 \times 10^{-5}$ M) in aqueous solution [3]. Tang et al. also reported that a tetrameric peptide, Ser-Pro-Gly-His, modified with a Fam selectively detected Cu^{2+} by fluorescence quenching through 1:1 binding ($K_d = 1.9 \times 10^{-6}$ M) in aqueous solution [4]. Meanwhile, Verma et al. reported that a dendritic hexameric peptide containing six His units selectively detected Cu^{2+} by fluorescence quenching in 50% aqueous methanol [5]. Moreover, Wu et al. reported that a trimeric peptide, Gly-Cys-Ala, modified with a Fam

detected Cu^{2+} or Ag^+ by fluorescence quenching through 2:1 binding ($K_d = 3.5 \times 10^{-14} \text{ M}^2$ for Cu^{2+} and $4.9 \times 10^{-14} \text{ M}^2$ for Ag^+) in aqueous solution [6]. Zang et al. also reported that a nonapeptide, His-Asp-Ser-Gly-Trp-Glu-Val-His-His, selectively detected Cu^{2+} by fluorescence quenching through 2:1 binding ($K_d = 5.8 \times 10^{-9} \text{ M}^2$) in aqueous solution [7]. Furthermore, Huang et al. reported that a hexameric peptide dimerized through disulfide binding containing two tetraphenylethylenes selectively detected Pb^{2+} by fluorescence emission through 1:1 binding ($K_d = 2.1 \times 10^{-6} \text{ M}$) in 20% aqueous acetonitrile [8]. Ramezanzpour et al. reported that trimeric Ser-Glu-Glu and heptameric Ala-Glu-Pro-Glu-Ala-Glu-Pro modified with a 2-aminobenzoyl group selectively detected Al^{3+} by fluorescence emission through 1:1 binding ($K_d = 7.7 \times 10^{-5}$ and $5.7 \times 10^{-5} \text{ M}$, respectively) in aqueous solution [9]. Li et al. reported that a pentameric peptide, Glu-Cys-Glu-Glu-Trp, modified with a dansyl group (Dns), selectively detected Ag^+ by ratiometric and turn-on fluorescence emission through 1:1 binding ($K_d = 6.4 \times 10^{-9} \text{ M}$) in aqueous solution [10]. Finally, Lee et al. reported that a decameric peptide, Ala-Ala-Cys-Ala-Ala-His-Cys-Trp-Ala-Glu, modified with a Dns, detected Cd^{2+} , Pb^{2+} , Zn^{2+} , or Ag^+ by ratiometric and turn-on fluorescence emission through 2:1 binding ($K_d = 2.6\text{--}4.5 \times 10^{-10} \text{ M}^2$) in aqueous solution [11].

The fluorescent peptide probes mentioned above are linear peptides, and there are concerns that the flexibility of their molecular chains causes low selectivity for metal ions and weak binding to such ions. To avoid this possibility, we have focused on conformationally restricted cyclic peptides as fluorescent metal ion sensors. Compared to linear peptides, cyclic peptides can be expected to improve specificity for targets due to their rigid conformation and to strongly bind to targets due to reduced entropy loss. For example, it has been reported that the cyclic version of cell-penetrating peptides (Tat and oligoarginine) [12,13] and a cell-adhesive (RGD) peptide [14] have better cellular uptake and cell-adhesive properties than the corresponding linear peptides, respectively.

In this study, we developed a water-soluble metal ion sensor based on a hexameric peptide incorporating fluorescent dyes, pyrenyl units (Pyr), which is expected to respond with fluorescence to binding with metal ions (Figure 1). For a similar cyclic peptide, Daub et al. reported that a hexameric cyclic peptide, -Gly-Gly-Pyr-Gly-Gly-Pyr-, selectively detected Ca^{2+} by Pyr-based excimer emission through 2:1 binding in 1,1,1,3,3,3-hexafluoro-2-propanol/methanol (=4/1 v/v) [15]. Unfortunately, this cyclic peptide was not detected in an aqueous solution due to its low water solubility. Low water solubility is a problem when using cyclic peptides as metal ion sensors, not limited to the cyclic peptides mentioned above [16]. Additionally, the introduction of His units into cyclic peptides is known to promote Cu^{2+} capture [17]. Based on the above design, the peptide in this study contains the following four moieties: (1) cyclic peptide for conformational restriction; (2) fluorescent dye pyrene for ion detection; (3) Arg unit for improved water solubility; and (4) His unit for specific ion capture.

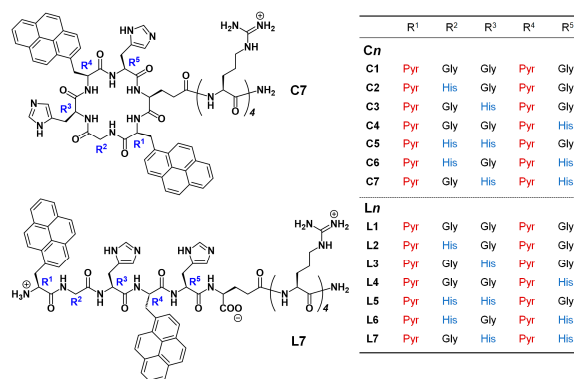


Figure 1. Chemical structures of cyclic peptides **Cn** ($n = 1\text{--}7$) and linear peptides **Ln** ($n = 1\text{--}7$). Left: Representative chemical structures of **Cn** (**C7**) and **Ln** (**L7**). Right: Pyr is introduced at R¹ and R⁴ in **Cn** and **Ln**. His or Gly is introduced at R², R³, or R⁵. **C2–C4** and **L2–L4** have one His introduced at different positions, and **C5–C7** and **L5–L7** have two His.

In this study, we used linear peptide and cyclic peptide sensors to assess their conformational effects through their fluorescent responses to metal ions. Furthermore, we investigated the details of the binding between a cyclic peptide containing two His units and Cu^{2+} ions, which were obtained by evaluating the fluorescence response of peptides to various metal ions.

2. Materials and Methods

2.1. Materials

9-Fluorenylmethyloxycarbonyl group (Fmoc)-derivatized amino acids, Fmoc-Glu-ODmab (Dmab; 4-[[1-(4,4-dimethyl-2,6-dioxocyclohexylidene)-3-methylbutyl]amino]benzyl group), Fmoc-derivatized super acid labile-poly(ethylene)glycol (Fmoc-NH-SAL-PEG) resin, piperidine, *O*-(1H-benzotriazol-1-yl)-*N,N,N',N'*-tetramethyluronium hexafluorophosphate (HBTU), *N*-methylmorpholine (NMM), trifluoroacetic acid (TFA), 1H-benzotriazol-1-ylxytripyrrolidinophosphonium hexafluorophosphate (PyBop), 1-hydroxybenzotriazole (HOBt), *N,N*-diisopropylethylamine (DIPEA), and triisopropylsilane (TIPS) were purchased from Watanabe Chemicals (Hiroshima, Japan). *N,N'*-Dimethylformamide (DMF), hydrazine, *N*-methyl-2-pyrrolidinone (NMP), methanol, diethyl ether, dichloromethane, 2-[4-(2-hydroxyethyl)-1-piperazinyl]ethanesulfonic acid (HEPES), and acetonitrile were purchased from FUJIFILM Wako Pure Chemical Corporation (Osaka, Japan). Seventeen metal ions used in this study were prepared by dissolving the following compounds in a buffer solution: barium chloride dihydrate (Ba^{2+}), cadmium chloride (Cd^{2+}), cerium(III) chloride (Ce^{3+}), cobalt(II) chloride hexahydrate (Co^{2+}), chromium(III) chloride hexahydrate (Cr^{3+}), copper(II) chloride dihydrate (Cu^{2+}), iron(III) chloride hexahydrate (Fe^{3+}), potassium chloride (K^+), magnesium chloride hexahydrate (Mg^{2+}), manganese(II) chloride tetrahydrate (Mn^{2+}), nickel(II) chloride hexahydrate (Ni^{2+}), lead(II) chloride (Pb^{2+}), and zinc chloride (Zn^{2+}) were purchased from Nacalai Tesque (Kyoto, Japan). Aluminum(III) chloride hexahydrate (Al^{3+}), calcium chloride dihydrate (Ca^{2+}), iron(II) chloride tetrahydrate (Fe^{2+}), and sodium chloride (Na^+) were purchased from FUJIFILM Wako Pure Chemical Corporation.

2.2. Peptide Synthesis

We prepared seven cyclic peptides **C1–C7** (Figure 1) using conventional Fmoc-based solid-phase peptide synthesis. Peptide cyclization was also performed on a solid support (Fmoc-NH-SAL-PEG resin containing 14.4 mmol of Fmoc on the resin surface) [18–20]. We deprotected an Fmoc group by reacting the resin with 20% piperidine in DMF for 7 min at room temperature, followed by washing seven times with DMF. Next, as a coupling process, the amino groups on the resin were reacted with 4.0 equivalents of Fmoc-derivatized amino acids, including Fmoc-Glu-ODmab, 3.6 equivalents of HBTU, and 11.5 equivalents of NMM in DMF for 40 min at room temperature, followed by washing four times with DMF. By repeating these deprotection and coupling processes, we extended a peptide with a predetermined sequence onto the resin. After completing the deprotection of an N-terminal amino acid unit, we deprotected a Dmab in a Glu-ODmab unit of the peptide by reacting with 3% hydrazine in DMF for 6 min at room temperature. After washing the resin five times with DMF, 10% DIPEA in DMF was added and stirred at room temperature for 10 min, followed by further washing three times with DMF, methanol, and then diethyl ether. Subsequently, we added 40 equivalents of DIPEA, 20 equivalents of PyBop, and 20 equivalents of HOBt in NMP and allowed coupling overnight at 60 °C. Through this process, an amide bond was formed between the carboxylic acid from which Dmab was deprotected and the amino group at the N-terminus, and the peptide was cyclized on the resin. In the case of synthesizing linear peptides **L1–L7**, after deprotecting Dmab as described above, the following cleavage process was performed without cyclization. We also generated peptides **C8–C16** and **L8–L16** (Figure S1), which contain Pyr at two different positions on the cyclic moiety, on the resin using the same process as described above.

After washing the resin with dichloromethane, 95% TFA, 2.5% water, and 2.5% TIPS were added and treated for 1.5 h at room temperature to cleave the peptide from the resin

and further deprotect the protecting groups on the amino acid side chains. The crude peptide was precipitated in diethyl ether and washed with diethyl ether until a neutral pH was reached. The peptides were purified using reverse-phase high-pressure liquid chromatography (RP-HPLC) on a C18 preparative column (Cadenza 5CD-C18; Imtakt, Kyoto, Japan). Final product identification was performed using matrix-assisted laser desorption/ionization-time-of-flight (MALDI-ToF) mass spectrometry (Shimadzu AXIMA Confidence, Shimadzu, Kyoto, Japan) (Figures S2–S5) and HPLC on a C18 analytical column (Cadenza CD-C18; Imtakt) (Figures S6–S9).

2.3. Fluorescence Spectrometry

Fluorescence spectra of all peptides were measured in aqueous buffer (100 mM HEPES, pH 7.0) at 25 °C using a JASCO FP-8200 fluorescence spectrometer. The excitation wavelength was 340 nm, and the emission wavelengths ranged from 350 nm to 600 nm. The path length of the quartz cuvette was 1 cm. Fluorescence spectra of **C1**, **C8–C16**, **L1**, and **L8–L16** (Figure S10) were measured at a concentration of 500 nM to investigate the monomer and excimer emission characteristics of the two Pyr units in the peptides. In the fluorescence spectra of **C1–C7** and **L1–L7** with 17 types of metal ions (Al^{3+} , Ba^{2+} , Ca^{2+} , Cd^{2+} , Ce^{3+} , Co^{2+} , Cr^{3+} , Cu^{2+} , Fe^{2+} , Fe^{3+} , K^+ , Mg^{2+} , Mn^{2+} , Na^+ , Ni^{2+} , Pd^{2+} , and Zn^{2+}), the final concentration of the peptide was 500 nM, and 100 equivalents (final concentration: 50 mM) of each metal ion was added to the peptide solution before incubation for 5 min and measurement of the fluorescence spectra (Figures S11 and S12). In the competition assay, 20 equivalents of each metal ion solution (final concentration: 10 mM) were added to **L1** and **C4–C7** solutions (final concentration: 500 nM), and the fluorescence spectra were measured after incubation for 5 min. Furthermore, 2 equivalents of a Cu^{2+} solution (final concentration: 1 mM) were added to the peptide solution (final concentration: 500 nM). After incubation for 1 h, 20 equivalents of a solution of each metal ion were added to the peptide (final concentration: 10 mM), and the fluorescence spectra were measured after incubation for 5 min. In the analysis using a Job plot, we prepared **C7** solution (1 mM) and a Cu^{2+} solution (1 mM) at different ratios [$\text{Cu}^{2+}/(\text{C7} + \text{Cu}^{2+}) = 0.0, 0.1, 0.2, 0.3, 0.4, 0.5, 0.6, 0.7, 0.8, \text{ and } 0.9$] and measured the fluorescence spectra after incubation for 5 min. The degree of quenching was estimated by multiplying the fluorescence intensity at 377 nm when the ratio was 0.0 (F_0) by the ratio of the peptide in the mixed solution [$1 - \text{Cu}^{2+}/(\text{C7} + \text{Cu}^{2+})$] and subtracting the fluorescence intensity at 377 nm obtained at each ratio (F). In the case of titration curves, the concentration of **C1–C7** was maintained at 500 nM, while the concentration of Cu^{2+} was varied in order to create peptide/ Cu^{2+} ratios of 0.0, 1.0, 2.0, 3.0, 4.0, 5.0, 6.0, 7.0, 8.0, and 10, or 0.0, 0.2, 0.4, 0.6, 0.8, 1.0, 1.2, 1.4, 1.6, 1.8, 2.0, 2.25, 2.5, 2.75, 3.0, 5.0, 7.5, and 10. The fluorescence spectra were measured after incubation of the peptide with Cu^{2+} for 5 min. Fluorescence titration curves were recorded based on fluorescence intensities at 377 nm.

The limit of detection was calculated by the result of a fluorescence titration curve of **C7** with Cu^{2+} from $3s/m$, where s is the standard deviation of this blank measurement, which was obtained by determining the fluorescence intensity of **C7** without Cu^{2+} , measured five times. m is the slope of the intensity at 377 nm versus the concentration of Cu^{2+} .

Equilibrium dissociation constants (K_d) were obtained by fitting the titration curve to the following equation [21,22]:

$$F = F_0 - (F_0 - F_s) \frac{(P_1 + P_2 + K_d) - \sqrt{(P_1 + P_2 + K_d)^2 - 4Pc}}{2P} \quad (1)$$

where F is the relative fluorescence intensity of **C7** when Cu^{2+} was added, F_0 is the predicted fluorescence intensity of **C7** at the initial concentration, F_s is the predicted fluorescence intensity at saturation, P_1 is the fixed concentration of **C7** (500 nM), P_2 is the concentration of Cu^{2+} at each point, and K_d is the dissociation constant of **C7**/ Cu^{2+} .

2.4. ESI Mass Spectrometry

For mass spectrometric analysis of the peptides, a G6520 Q-TOF mass spectrometer (Agilent, Santa Clara, CA, USA) equipped with an electrospray ionization (ESI) source was used. Data were acquired in positive mode. A water/acetonitrile solution (25/75 v/v%) containing 0.5 μM peptide and 10 μM metal ions (Cu^{2+} , Mg^{2+} , or Ni^{2+}) was injected with a syringe pump (0.1 mL/min). The compound qualification conditions were as follows: gas temperature, 325 $^{\circ}\text{C}$; capillary voltage, 3500 V; and fragmentor voltage, 175 V. Data acquisition was performed using MassHunter Acquisition workstation software (Agilent), and raw data files were analyzed and deconvoluted using MassHunter Qualitative Analysis B.07.00 software (Agilent).

2.5. Cyclic Voltammetry

We investigated whether the behavior of electron transfer in the peptides was affected by the addition of metal ions. A three-electrode electrochemistry cell was fabricated using a beaker with a solution volume of ~ 3 mL. A bundle (diameter: ~ 1 mm) of long carbon nanotubes (CNTs) with a length of ~ 1 cm (weight: ~ 0.3 mg) was used as a working electrode without any treatment [23]. Pt wire and Ag/AgCl (3 M KCl) were used as a counter electrode and a reference electrode, respectively. Sample solutions with different concentrations of peptides and Cu^{2+} were prepared with an electrolyte (0.1 M KCl). The potential was swept using a potentiostat (HZ-7000; Hokuto Denko, Tokyo, Japan) from -0.5 to 0.6 V for several cycles with a scan rate of 20 mV s^{-1} .

3. Results and Discussion

3.1. Design of Pyr-Labeled Peptides

We designed and synthesized 14 peptides, **C1–C7** and **L1–L7**, for the detection of specific metal ions in water via the fluorescent dye Pyr (Figure 1). **C1–C7** contain a hexameric cyclic peptide moiety, and **L1–L7** are their linear equivalents. These peptides contain multiple (two) Pyr units in the first (R^1) and fourth (R^4) positions. We attempted to synthesize cyclic peptides containing one Pyr but were unable to obtain them because they were more difficult to purify than cyclic peptides containing two Pyr units. **C1–C7** and **L1–L7** also contain a “tail” of four Arg units to confer water solubility. Based on the sequence of the cyclic peptide moiety of **C1**, one or two of the Gly units are replaced by His units in **C2–C7**. It is known that His units have high binding affinity for specific ions [3–5,7,11,17]. Prior to using these peptides, we synthesized nine cyclic peptides **C8–C16** (Figure S1) with different positions of the two Pyr units in the cyclic peptide moiety in **C1**. The fluorescence profile of these cyclic peptides depended on the position of Pyr (Figure S10a). Its dependence was also observed for the linear peptides **L8–L16** (Figure S1) corresponding to each cyclic peptide (Figure S10b). We thought that excimer formation between Pyr in the molecule would hinder fluorescence assessment, so we selected **C1** (Pyr at R^1 and R^4 positions) for this study because it enables monomer emission fluorescence to be more exclusively obtained.

3.2. Fluorescence Detection of Metal Ions for C1 and L1

We first investigated whether the fluorescence of the cyclic peptide **C1** was affected by the addition of metal ions. Figure 2a shows the fluorescence spectra of **C1** when Mg^{2+} or Cu^{2+} were added. **C1** alone (black line) showed fluorescence derived from the pyrene monomer at 377 and 397 nm, and weak fluorescence derived from the pyrene excimer around 485 nm. This profile remained unchanged upon the addition of 100 equivalents of Mg^{2+} or Cu^{2+} relative to **C1** (blue and red lines, respectively). This shows that these metal ions do not affect the fluorescence emission of **C1**.

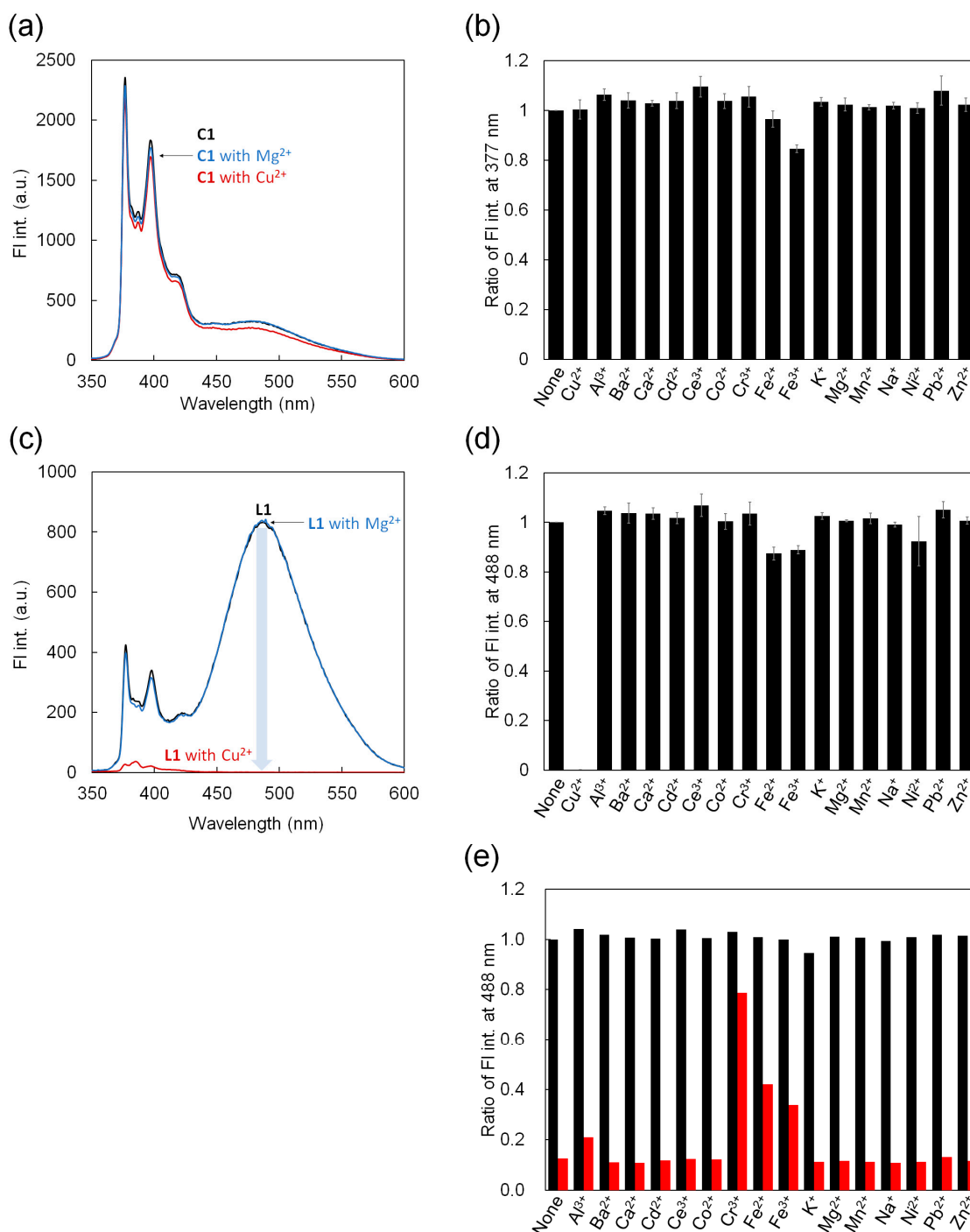


Figure 2. (a) Fluorescence spectra of C1 (500 nM) with Mg²⁺ and Cu²⁺ (100 equivalents to C1) in aqueous solution. (b) Fluorescence intensities at 377 nm of C1 with 17 metal ions. (c) Fluorescence spectra of L1 (500 nM) with Mg²⁺ and Cu²⁺ (100 equivalents to L1) in aqueous solution. (d) Fluorescence intensities at 488 nm of L1 with 17 metal ions. (e) Competition assay of Cu²⁺ against other ions by L1. Black bars indicate an aqueous L1 solution (500 nM) containing 20 equivalents of each metal ion. Red bars indicate an aqueous L1 solution (500 nM) in which 20 equivalents of each metal ion were added after adding 2 equivalents of Cu²⁺.

We further measured the fluorescence spectra of C1 when 15 types of metal ions other than Mg²⁺ and Cu²⁺ were added (Figure S11). Figure 2b shows the fluorescence intensity at 377 nm based on the spectra obtained by adding 100 equivalents of 17 metal ions (Cu²⁺, Al³⁺, Ba²⁺, Ca²⁺, Cd²⁺, Ce³⁺, Co²⁺, Cr³⁺, Fe²⁺, Fe³⁺, K⁺, Mg²⁺, Mn²⁺, Na⁺, Ni²⁺, Pd²⁺, and

Zn²⁺). The results showed that the intensities were the same as those of **C1** alone. This reveals that, within the range of metal ions that we investigated, **C1** does not show any fluorescence response even when metal ions are added. **C1** is identical to a cyclic peptide developed by Daub et al. [15], except that **C1** has an Arg tail attached. Daub's cyclic peptide exhibited an excimer fluorescence response when sandwiched with Ca²⁺ in an organic solvent. Although the presence of the Arg units must be taken into account, our results indicate that, in water, it is difficult for this hexameric cyclic peptide moiety to respond fluorescently not only to Ca²⁺ but also to many metal ions, probably due to the interference of water molecules.

We similarly investigated the fluorescence emission of **L1**, a linear version of **C1**. Figure 2c shows the fluorescence spectra of **L1** with Mg²⁺ or Cu²⁺. **L1** alone (black line) showed fluorescence from the pyrene monomer as well as strong fluorescence from the pyrene excimer at 488 nm. This strong excimer fluorescence was not observed for **C1**. These spectra should reflect the difference in molecular flexibility between **C1** and **L1**. Even when Mg²⁺ was added to **L1** (blue line), its fluorescence profile did not change. Meanwhile, interestingly, the addition of Cu²⁺ (red line) significantly affected the fluorescence response of **L1** and decreased the fluorescence intensity across the spectrum.

The fluorescence intensity at 488 nm based on the spectra of 100 equivalents of the 17 metal ions (Figure S12) showed that this fluorescence response only occurred with Cu²⁺ (Figure 2d).

To investigate in detail the fluorescence quenching of **L1** by Cu²⁺, we performed a competition assay of Cu²⁺ against other ions (Figure 2e). First, when 20 equivalents of each metal ion to **L1** except Cu²⁺ were added to the **L1** solution, the fluorescence intensity at 488 nm showed no fluorescence quenching (black bars), similar to the result in Figure 2d. Next, when 2 equivalents of Cu²⁺ and 20 equivalents of each metal ion were added in the **L1** solution, the intensities showed quenching for many metal ions, comparable to the decrease in fluorescence caused by the addition of only Cu²⁺ (mean of ~88% quenching; red bars). However, it was found that Cr³⁺, Fe²⁺, and Fe³⁺ suppressed the fluorescence quenching (24%, 58%, and 66% quenching, respectively). These results suggest that the interaction of **L1** with Cu²⁺ can be visualized through fluorescence quenching, that is, the detection of Cu²⁺ through the fluorescence quenching of **L1**. Meanwhile, unfortunately, the interaction between **L1** and Cu²⁺ is hindered when Cr³⁺, Fe²⁺, and Fe³⁺ coexist in the solution, indicating that Cu²⁺-selective fluorescence detection by **L1** is difficult. It is also seen that metal ions such as Cr³⁺, Fe²⁺, and Fe³⁺ do not exhibit a fluorescent response even when they interact with **L1**.

3.3. Fluorescence Detection of Metal Ions for C2–C7 and L2–L7 Containing Histidine Units

We also assessed the fluorescence emission of His-containing **C2–C7** and **L2–L7** peptides for the 17 metal ions as in Section 3.2. Figure 3a shows the fluorescence intensity at 377 nm of the fluorescence spectra of **C2–C7** (Figure S11) when four representative metal ions (Cu²⁺, Co²⁺, Mg²⁺, and Ni²⁺) are added. The results indicated that **C1** showed no fluorescence response to the addition of any metal ions, including Cu²⁺ (Figure 2b), while **C2–C7** showed fluorescence quenching only when Cu²⁺ was added. This indicates that the introduction of His units in the cyclic peptide moiety of **C2–C7** contributes to the interaction with Cu²⁺. In other words, it was suggested that introducing His units into the cyclic peptide could enable the specific detection of Cu²⁺.

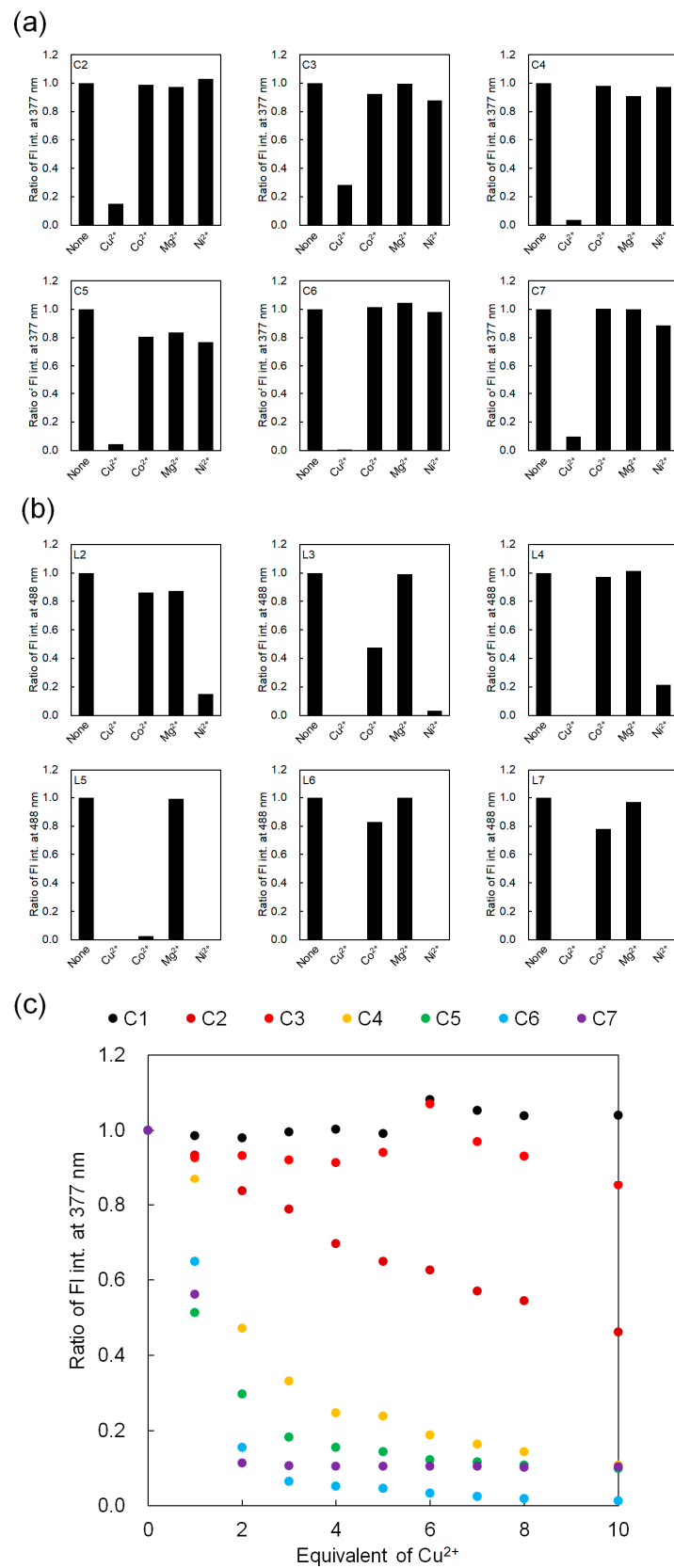


Figure 3. Fluorescence intensities at 377 nm of (a) C2–C7 and 488 nm of (b) L2–L7 with representative metal ions (Cu²⁺, Co²⁺, Mg²⁺, and Ni²⁺). (c) Fluorescence titration curves at 377 nm derived from pyrene monomer emission in C1–C7 (500 nM constant) with Cu²⁺.

Meanwhile, Figure 3b shows the fluorescence intensity at 488 nm of the fluorescence spectra of L2–L7 (Figure S12) when metal ions were added. L1 showed fluorescence quenching only when Cu^{2+} was added (Figure 2d), but L2, L4, L6, and L7 showed fluorescence quenching when not only Cu^{2+} but also Ni^{2+} was added, and L3 and L5 also showed the quenching when Cu^{2+} , Co^{2+} , and Ni^{2+} were added. Such sequence-specific metal ion selectivity of peptides has also been reported for water-soluble peptoid chelators by Maayan et al. [24] These results demonstrate that the introduction of His units into the flexible linear peptide compared with the cyclic peptide caused quenching due to interaction with multiple metal ions other than Cu^{2+} .

In the assessment of fluorescence quenching of the peptide described above, 100 equivalents of each metal ion were added to the peptides, but here we investigated the fluorescence response of the peptide to Cu^{2+} with an even lower number of equivalents. Figure 3c shows the change in fluorescence intensity at 377 nm when 0–10 equivalents of Cu^{2+} ions were added to C1–C7. Their fluorescence spectra are shown in Figure S13. As expected, C1 did not exhibit fluorescence quenching upon the addition of Cu^{2+} within this range. Similarly, C3 (His = R²) did not exhibit fluorescence quenching. C2 (His = R³) caused fluorescence quenching as the amount of Cu^{2+} increased, but the change was gradual. However, it was found that, for the four cyclic peptides C4–C7, fluorescence quenching occurred rapidly from zero to two equivalents, and the quenching was almost saturated after two equivalents. The degree of quenching was in the following order: C4 (His = R⁵) < C5 (His = R² and R³) < C6 (His = R² and R⁵) = C7 (His = R³ and R⁵). This indicates that the binding affinity between Cu^{2+} and the cyclic peptides depends on the number and position of His units in the cyclic peptide. This also indicates that C4–C7, especially C6 and C7, can strongly detect Cu^{2+} through fluorescence quenching; that is, these peptides strongly interact with Cu^{2+} . Therefore, as described in the next section, we focused on C7 and investigated its fluorescence emission for each metal ion in the same manner as described in Section 3.2.

3.4. Fluorescence Detection of Metal Ions for C7 and L7

We investigated whether the fluorescence of C7 was affected by the addition of metal ions. Figure 4a shows the fluorescence spectra of C7 with Mg^{2+} or Cu^{2+} . For C7 alone and upon the addition of Mg^{2+} (black and blue lines, respectively), the findings revealed fluorescence derived from the pyrene monomer and the weak pyrene excimer. However, the addition of Cu^{2+} (a red line) caused a significant decrease in the fluorescence of C7. These results are consistent with those in Figure 3a.

We further measured the fluorescence spectra of C7 with 17 metal ions (Figure S11). Figure 4b shows the fluorescence intensity at 377 nm based on the spectra obtained by adding 100 equivalents of the 17 metal ions, indicating that this fluorescence response only occurred with Cu^{2+} .

To investigate in detail the fluorescence quenching of C7 by Cu^{2+} , we performed competition assays of Cu^{2+} against other ions (Figure 4c). First, when 20 equivalents of each metal ion other than Cu^{2+} were added to C7, the fluorescence intensity at 377 nm was similar to the result in Figure 4b, that is, no fluorescence quenching was observed (black bars). Then, when 2 equivalents of Cu^{2+} and 20 equivalents of each metal ion were added to C7, the fluorescence showed quenching for all metal ions, comparable to the decrease in fluorescence due to the addition of Cu^{2+} alone (red bars). These results reveal that, among the metal ions used, C7 selectively detects Cu^{2+} through fluorescence quenching. We also performed competition assays for C4–C6, which showed good binding affinity for Cu^{2+} similar to that for C7 (Figure S14). Their fluorescence spectra are shown in Figure S15. Interestingly, C5 (His = R² and R³) showed selectivity of fluorescence response to Cu^{2+} , similar to C7 (His = R³ and R⁵), but C4 (His = R⁵) and C6 (His = R² and R⁵) showed no selectivity, and fluorescence quenching was hindered by Cr^{3+} , Fe^{2+} , and Fe^{3+} . These results indicate that the position of His in the cyclic peptide moiety influences its selectivity. Together with the results in Figure 3c, we concluded that, in this cyclic peptide, the presence

of two His units and the His unit at R⁵ increase the binding affinity for Cu²⁺ and that the presence of a His unit at R³ confers selectivity of the fluorescence response to Cu²⁺.

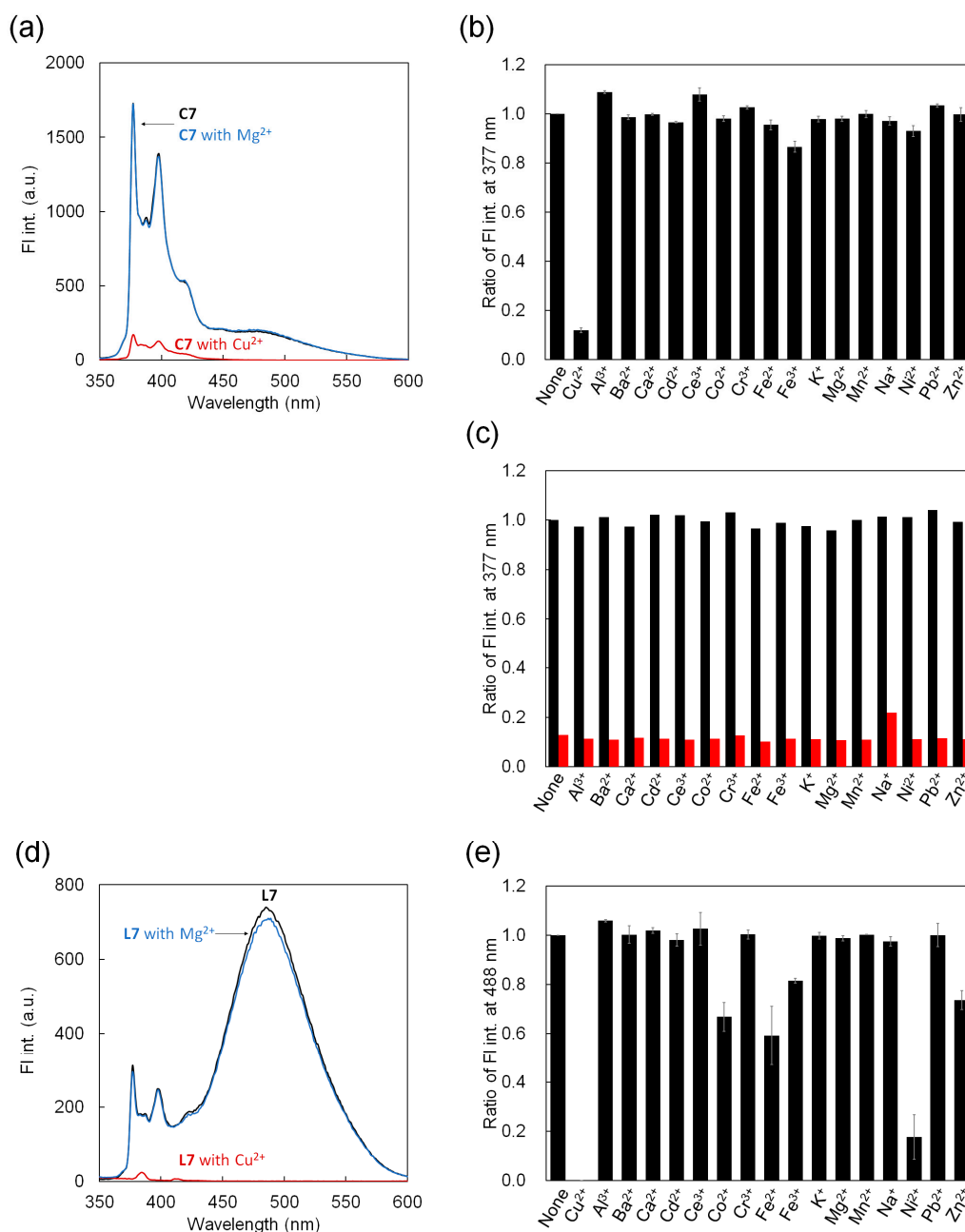


Figure 4. (a) Fluorescence spectra of C7 (500 nM) with Mg²⁺ or Cu²⁺ (100 equivalents to C7) in aqueous solution. (b) Fluorescence intensities at 377 nm of C7 with 17 metal ions. (c) Competition assay of Cu²⁺ against other ions by C7. Black bars indicate an aqueous C7 solution (500 nM) containing 20 equivalents of each metal ion. Red bars indicate an aqueous C7 solution (500 nM) in which 20 equivalents of each metal ion were added after adding 2 equivalents of Cu²⁺. (d) Fluorescence spectra of L7 (500 nM) with Mg²⁺ or Cu²⁺ (100 equivalents to L7) in aqueous solution. (e) Fluorescence intensities at 488 nm of L7 with 17 metal ions.

We similarly investigated the fluorescence emission of L7, the linear equivalent of C7. Figure 4d shows the fluorescence spectra of L7 with Mg²⁺ or Cu²⁺. L7 alone (black line) showed fluorescence from the pyrene excimer and monomer, similar to that of L1 (Figure 2c). The addition of Mg²⁺ did not change the fluorescence profile (blue line);

meanwhile, the addition of Cu^{2+} produced spectrum-wide fluorescence quenching (red line). This result is similar to those of **L1** and **C7**.

However, the fluorescence intensity at 488 nm based on the fluorescence spectra of 100 equivalents of 17 metal ions showed that this fluorescence quenching occurred not only for Cu^{2+} but also for Ni^{2+} and, to a lesser extent, for Co^{2+} and Fe^{2+} (Figure 4e). These results indicate that peptide cyclization is important for the selective fluorescence detection of Cu^{2+} by these peptides. Presumably, structural restriction of the molecule by cyclization promotes interaction between the peptides and a specific metal ion.

3.5. A 1:1 interaction between **C7** and Cu^{2+}

In previous sections, we showed that **C7** selectively detects Cu^{2+} through fluorescence quenching. Finally, we investigated the interaction between **C7** and Cu^{2+} in detail. Figure 5a shows a fluorescence Job plot of Cu^{2+} versus **C7**, and their fluorescence spectra are shown in Figure S16. When Cu^{2+} was added at a ratio from 0.0 to 0.4, the degree of quenching of **C7** increased, and when Cu^{2+} was added at a ratio from 0.6 to 0.9, the degree decreased. This shows that the degree of fluorescence quenching is greatest when **C7** and Cu^{2+} are mixed at a 1:1 ratio, indicating their interaction at this ratio.

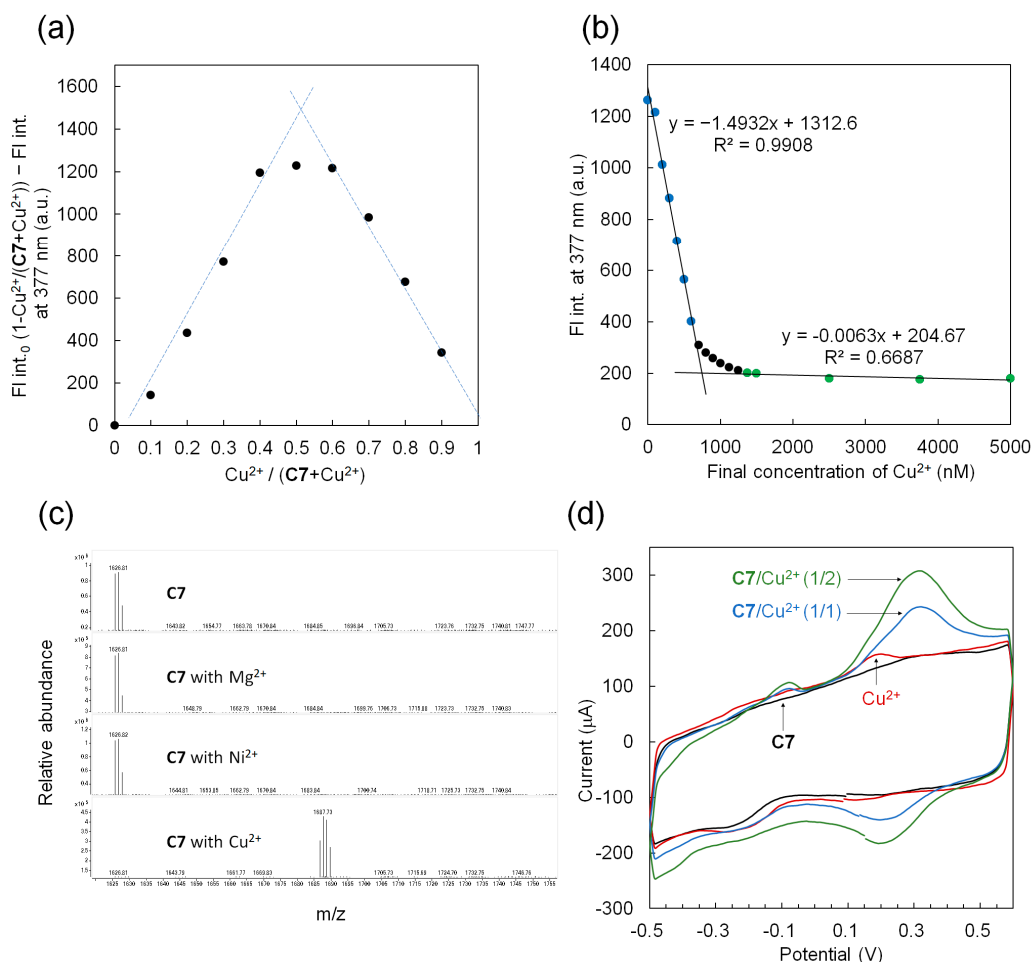


Figure 5. (a) Fluorescence Job plot of **C7** with Cu^{2+} . (b) Fluorescence titration curve at 377 nm of **C7** (500 nM constant) by Cu^{2+} in aqueous solution. (c) ESI-mass spectra of **C7** with and without 20 equivalents of each metal ion (Mg^{2+} , Ni^{2+} , and Cu^{2+}). (d) Cyclic voltammetry of **C7** (250 μM) and Cu^{2+} with different concentrations.

Figure 5b shows a fluorescence titration curve when a given concentration of Cu^{2+} (0–10 equivalents to **C7**; 0–5000 nM) was added to **C7** (500 nM constant). The correspond-

ing fluorescence spectra are shown in Figure S17. The results revealed that, at a lower Cu^{2+} concentration (0–600 nM), the fluorescence intensity at 377 nm decreased rapidly. Meanwhile, at a higher Cu^{2+} concentration (1375–5000 nM), the fluorescence quenching was saturated. This is consistent with the results shown in Figure 3c. The lines obtained from the lower- and higher-concentration regions of Cu^{2+} intersect at 745 nM, indicating that **C7** and Cu^{2+} interact at a nearly 1:1 ratio, supporting the results in Figure 5a. We also calculated the dissociation constant (K_d) of **C7** and Cu^{2+} using Equation 1 from Figure 5b and obtained a value of 5.0×10^{-8} M. This value is smaller than that of His-Gly-Gly-Gly ($K_d = 3.7 \times 10^{-5}$ M) [3] and that of Ser-Pro-Gly-His ($K_d = 1.9 \times 10^{-6}$ M) [4] for Cu^{2+} mentioned above, indicating high binding affinity for Cu^{2+} due to structural restriction of **C7**. We further calculated the limit of detection from the line obtained from the low-concentration region of Cu^{2+} and found it to be 40 nM. This value is also smaller than that of His-Gly-Gly-Gly for Cu^{2+} mentioned above (3.9 mM), which is considered to be due to the high binding affinity of **C7** for Cu^{2+} .

Figure 5c shows the ESI mass spectra of **C7** when metal ions (Mg^{2+} , Ni^{2+} , and Cu^{2+}) were added. The main mass peak of **C7** was 1626.81, which showed good agreement with the theoretical value of 1626.80. In addition, only the same mass peak was detected in ESI mass spectra when 20 equivalents of Mg^{2+} or Ni^{2+} were added to **C7**, indicating that **C7** does not bind to Mg^{2+} or Ni^{2+} as indicated in Figure 3a. Meanwhile, in the ESI mass spectrum, when 20 equivalents of Cu^{2+} were added to **C7**, the mass peak corresponding to **C7** completely disappeared and a new peak appeared at 1687.73, which indicates a 1:1 binding of Cu^{2+} and **C7** (theoretical value when two H atoms are replaced by one Cu^{2+} in **C7** [25,26]: 1687.73). In addition, no peaks reflecting the binding of **C7** to multiple Cu^{2+} ions were observed. We also measured the ESI mass spectra of **C1** and **L7** mixed with the metal ions (Figure S18). The results showed that, for **C1**, no matter which metal ion was added, only a mass peak indicating **C1** was confirmed. In contrast, for **L7**, a mass peak was observed in which not only Cu^{2+} but also Ni^{2+} were bound to **L7** at a 1:1 ratio. Furthermore, for **L7**, a mass peak reflecting binding to Cu^{2+} at a 1:2 ratio was also confirmed. These results support Figure 3a and further highlight that **C7** and Cu^{2+} bind at a 1:1 ratio.

Figure 5d shows the results of cyclic voltammetry in an aqueous solution containing **C7** (250 μM) and Cu^{2+} at different concentrations. For **C7** alone (black curve), no current peak was observed within the measured potential range (−0.5 to 0.6 V). In addition, for Cu^{2+} alone (500 μM , red curve), a current peak at approximately 150 μA was observed around 0.2 V. This oxidation current came from the reaction between Cu^+ and Cu^{2+} . Meanwhile, in the mixed solution of **C7** and Cu^{2+} (**C7**: Cu^{2+} = 1:1 (blue curve) and 1:2 (green curve)), in addition to the shoulder current peak around 0.2 V, a significant current peak appeared around 0.33 V. This suggests that the potential of the $\text{Cu}^{2+}/\text{Cu}^+$ oxidation peak was shifted by **C7**. This is thought to be due to the different state of Cu^{2+} in the solution, and it is suggested that Cu^{2+} forms a complex with **C7**. In addition, the higher current peak value of Cu^{2+} in the presence of **C7** suggests that complex formation between **C7** and Cu^{2+} increased the amount of Cu^{2+} around the electrode, resulting in amplification of the peak current. This is possibly because the affinity between the complex and the CNT electrode is higher than that between Cu^{2+} and the CNT electrode. This is also supported by the fact that a higher concentration of Cu^{2+} increases the peak current value (green curve).

4. Conclusions

In this study, we used linear peptide and cyclic peptide sensors to assess their conformational effects through their fluorescent responses to metal ions and investigated the details of the binding between a cyclic peptide containing two His/Pyr units and Cu^{2+} ions, which were obtained by the assessment. We revealed that the hexameric cyclic peptide specifically binds Cu^{2+} at a 1:1 ratio, resulting in fluorescence quenching. In other words, this quenching allows the peptide to fluorescently detect Cu^{2+} . The introduction of two His units into the cyclic peptide, as well as the presence of His units at positions R⁵ and R³, is important for the binding affinity and selectivity of this peptide to Cu^{2+} , respectively,

probably giving a suitable multipoint interaction between them. While linear peptides bind Cu^{2+} , they also appear to bind other metal ions. In addition, the linear peptides appeared to bind not only to one Cu^{2+} ion but also to multiple Cu^{2+} ions. These results reveal that appropriate structural restriction, such as peptide cyclization, is required for the peptide to selectively and strongly bind to Cu^{2+} at a 1:1 ratio. Unfortunately, we are unable to propose a plausible complex structure between the cyclic peptide and Cu^{2+} ion due to the lack of information on crystalline structure and molecular simulation in this study. However, the present results will provide important insights for the development of peptide-based metal ion sensors.

In this study, we showed that the limit of detection of **C7** for Cu^{2+} is on the order of 10^{-8} M. According to the World Health Organization, the upper safe limit for Cu^{2+} in drinking water is 2 mg/L (3.2×10^{-5} M) [27]. In addition, blood-free copper in patients with Wilson's disease (a congenital genetic disease in which Cu^{2+} ingested through the diet is not normally excreted from the liver into the bile and intestinal tract and instead accumulates in the viscera, brain, and kidneys, causing severe damage to the liver and nerves) is usually 20–25 mg/dL ($3\text{--}4 \times 10^{-6}$ M) or higher, and 24 h urinary copper is usually 100 mg/24 h (1×10^{-6} M) or more [28–30]. These values suggest that **C7** could be used for monitoring Cu^{2+} in waterbodies and for diagnosing Wilson's disease.

In future work, we will develop peptides that can selectively bind to metal ions other than Cu^{2+} by changing the amino acid sequence within this cyclic peptide.

Supplementary Materials: The following supporting information can be downloaded at: <https://www.mdpi.com/article/10.3390/pr12040746/s1>, Figure S1: Chemical structures of **C8–C16** and **L8–L16**, Figure S2: MALDI-ToF mass spectra of **C1–C7**, Figure S3: MALDI-ToF mass spectra of **L1–L7**, Figure S4: MALDI-ToF mass spectra of **C8–C16**, Figure S5: MALDI-ToF mass spectra of **L8–L16**, Figure S6: HPLC chromatograms of **C1–C7**, Figure S7: HPLC chromatograms of **L1–L7**, Figure S8: HPLC chromatograms of **C8–C16**, Figure S9: HPLC chromatograms of **L8–L16**, Figure S10: Fluorescence spectra of **C1**, **C8–C16**, **L1**, and **L8–L16**, Figure S11: Fluorescence spectra of **C1–C7** with each 17 metal ion, Figure S12: Fluorescence spectra of **L1–L7** with each 17 metal ion, Figure S13: Fluorescence spectra of **C1–C7** for titration curves, Figure S14: Competition assay of **C4–C6**, Figure S15: Fluorescence spectra of **L1** and **C4–C7** for competition assay, Figure S16: Fluorescence spectra of **C7** with Cu^{2+} for Job's plot, Figure S17: Fluorescence spectra of **C7** for titration curve, and Figure S18: ESI mass spectra of **C1** and **L7** with and without Mg^{2+} , Ni^{2+} , and Cu^{2+} .

Author Contributions: Conceptualization, M.K.; methodology, M.K. and S.S.; formal analysis, Y.M. and M.K.; investigation, Y.M., S.S., R.F., Y.F. and H.S.; resources, H.S., T.O. and M.K.; data curation, Y.M. and M.K.; writing—original draft preparation, Y.M. and M.K.; writing—review and editing, H.S. and T.O.; visualization, Y.M., S.S. and M.K.; supervision, H.S., T.O. and M.K.; project administration, M.K.; funding acquisition, M.K. All authors have read and agreed to the published version of the manuscript.

Funding: This research received no external funding.

Data Availability Statement: The data presented in this study are available on request from the corresponding author.

Acknowledgments: The authors thank Tsugumi Shiokawa at the Division of Instrumental Analysis, Okayama University, for their assistance in mass spectrometry.

Conflicts of Interest: The funders had no role in the design of the study; in the collection, analyses, or interpretation of data; in the writing of the manuscript; or in the decision to publish the results.

References

1. Izatt, R.M.; Pawlak, K.; Bradshaw, J.S.; Bruening, R.L. Thermodynamic and Kinetic Data for Macrocyclic Interactions with Cations and Anions. *Chem. Rev.* **1991**, *91*, 1721–2085. [[CrossRef](#)]
2. Wu, D.; Sedgwick, A.C.; Gunnlaugsson, T.; Akkaya, E.U.; Yoon, J.; James, T.D. Fluorescent Chemosensors: The Past, Present and Future. *Chem. Soc. Rev.* **2017**, *46*, 7105–7123. [[CrossRef](#)]
3. Wu, S.-P.; Liu, S.-R. A New Water-Soluble Fluorescent Cu(II) Chemosensor Based on Tetrapeptide histidyl-glycyl-glycyl-glycine (HGGG). *Sens. Actuators B Chem.* **2009**, *141*, 187–191. [[CrossRef](#)]

4. Wang, P.; Wu, J.; Di, C.; Zhou, R.; Zhang, H.; Su, P.; Xu, C.; Zhou, P.; Ge, Y.; Liu, W.; et al. A Novel Peptide-based Fluorescence Chemosensor for Selective Imaging of Hydrogen Sulfide Both in Living Cells and Zebrafish. *Biosens. Bioelectron.* **2017**, *92*, 602–609. [[CrossRef](#)]
5. Ghosh, S.; Singh, P.; Verma, S. Morphological Consequences of Metal Ion–Peptide Vesicle Interaction. *Tetrahedron* **2008**, *64*, 1250–1256. [[CrossRef](#)]
6. Xu, J.; Liu, N.; Hao, C.; Han, Q.; Duan, Y.; Wu, J. A Novel Fluorescence “On-Off-On” Peptide-based Chemosensor for Simultaneous Detection of Cu^{2+} , Ag^+ and S^{2-} . *Sens. Actuators B Chem.* **2019**, *280*, 129–137. [[CrossRef](#)]
7. Zhang, Y.; Cai, Y.; He, Y.; Lin, Q.; Ren, J.; Cao, D.; Zhang, L. A Label-free Fluorescent Peptide Probe for Sensitive and Selective Determination of Copper and Sulfide Ions in Aqueous Systems. *RSC Adv.* **2021**, *11*, 7426–7435. [[CrossRef](#)]
8. Gui, S.; Huang, Y.; Zhu, Y.; Jin, Y.; Zhao, R. Biomimetic Sensing System for Tracing Pb^{2+} Distribution in Living Cells Based on the Metal–Peptide Supramolecular Assembly. *ACS Appl. Mater. Interfaces* **2019**, *11*, 5804–5811. [[CrossRef](#)]
9. Ramezanpour, S.; Barzinmehr, H.; Shiri, P.; Meier, C.; Ayatollahi, S.A.; Mehrazar, M. Highly Selective Fluorescent Peptide-based Chemosensors for Aluminium Ions in Aqueous Solution. *Anal. Bioanal. Chem.* **2021**, *413*, 3881–3891. [[CrossRef](#)] [[PubMed](#)]
10. Yu, S.; Wang, Z.; Gao, L.; Zhang, B.; Wang, L.; Kong, J.; Li, L. A Highly Selective and Sensitive Peptide-Based Fluorescent Ratio Sensor for Ag^+ . *J. Fluoresc.* **2021**, *31*, 237–246. [[CrossRef](#)] [[PubMed](#)]
11. Joshi, B.P.; Park, J.; Lee, W.I.; Lee, K.-H. Ratiometric and Turn-on Monitoring for Heavy and Transition Metal Ions in Aqueous Solution with a Fluorescent Peptide Sensor. *Talanta* **2009**, *78*, 903–909. [[CrossRef](#)]
12. Nischan, N.; Herce, H.D.; Natale, F.; Bohlke, N.; Budisa, N.; Cardoso, M.C.; Hackenberger, C.P.R. Covalent Attachment of Cyclic TAT Peptides to GFP Results in Protein Delivery into Live Cells with Immediate Bioavailability. *Angew. Chem. Int. Ed.* **2015**, *54*, 1950–1953. [[CrossRef](#)]
13. Qian, Z.; Martyna, A.; Hard, R.L.; Wang, J.; Appiah-Kubi, G.; Coss, C.; Phelps, M.A.; Rossman, J.S.; Pei, D. Discovery and Mechanism of Highly Efficient Cyclic Cell-Penetrating Peptides. *Biochemistry* **2016**, *55*, 2601–2612. [[CrossRef](#)] [[PubMed](#)]
14. Yamada, T.; Uyeda, A.; Kidera, A.; Kikuchi, M. Functional Analysis and Modeling of a Conformationally Constrained Arg-Gly-Asp Sequence Inserted into Human Lysozyme. *Biochemistry* **1994**, *33*, 11678–11683. [[CrossRef](#)]
15. Strauss, J.; Daub, J. Optically Active Cyclic Hexapeptides with Covalently Attached Pyrene Probes: Selective Alkaline Earth Metal Ion Recognition Using Excimer Emission. *Org. Lett.* **2002**, *4*, 683–686. [[CrossRef](#)]
16. Gahan, L.R.; Cusack, R.M. Metal Complexes of Synthetic Cyclic Peptides. *Polyhedron* **2018**, *153*, 1–23. [[CrossRef](#)]
17. Kotynia, A.; Pap, J.; Brasun, J. The Binding Abilities of Homodetic Cyclic His-Peptides toward Copper Ions. *Inorganica Chim. Acta* **2018**, *472*, 3–11. [[CrossRef](#)]
18. Qin, C.; Xu, C.; Zhang, R.; Niu, W.; Shang, X. On-resin Cyclization and Antimicrobial Activity of Laterocidin and Its Analogues. *Tetrahedron Lett.* **2010**, *51*, 1257–1261. [[CrossRef](#)]
19. Berthelot, T.; Gonçalves, M.; Lain, G.; Estieu-Gionnet, K.; Déléris, G. New Strategy towards the Efficient Solid Phase Synthesis of Cyclopeptides. *Tetrahedron* **2006**, *62*, 1124–1130. [[CrossRef](#)]
20. Johnson, T.; Liley, M.; Cheeseright, T.J.; Begum, F. Problems in the Synthesis of Cyclic Peptides through Use of the Dmab Protecting Group. *J. Chem. Soc. Perkin Trans.* **2000**, *1*, 2811–2820. [[CrossRef](#)]
21. Sgolastra, F.; Backlund, C.M.; Ozay, I.E.; deRonde, B.M.; Minter, L.M.; Tew, G.N. Sequence Segregation Improves Non-Covalent Protein Delivery. *J. Control. Release* **2017**, *254*, 131–136. [[CrossRef](#)] [[PubMed](#)]
22. Heitz, F.C.; Morris, M.C.; Fesquet, D.; Cavadore, J.; Dorée, M.; Divita, G. Interactions of Cyclins with Cyclin-Dependent Kinases: A Common Interactive Mechanism. *Biochemistry* **1997**, *36*, 4995–5003. [[CrossRef](#)] [[PubMed](#)]
23. Sugime, H.; Sato, T.; Nakagawa, R.; Hayashi, T.; Inoue, Y.; Noda, S. Ultra-Long Carbon Nanotube Forest via *in Situ* Supplements of Iron and Aluminum Vapor Sources. *Carbon* **2021**, *172*, 772–780. [[CrossRef](#)]
24. Ghosh, P.; Rosenberg, I.; Maayan, G. Sequence-function Relationship within Water-soluble Peptoid Chelators for Cu^{2+} . *J. Inorg. Biochem.* **2021**, *217*, 111388–111394. [[CrossRef](#)]
25. Bar-Or, D.; Curtis, G.; Rao, N.; Bampos, N.; Lau, E. Characterization of the Co^{2+} and Ni^{2+} Binding Amino-acid Residues of the N-Terminus of Human Albumin. *Eur. J. Biochem.* **2001**, *268*, 42–47. [[CrossRef](#)] [[PubMed](#)]
26. Cho, Y.; Mirzapour-Kouhdasht, A.; Yun, H.; Park, J.H.; Min, H.J.; Lee, C.W. Development of Cobalt-Binding Peptide Chelate from Human Serum Albumin: Cobalt-Binding Properties and Stability. *Int. J. Mol. Sci.* **2022**, *23*, 719. [[CrossRef](#)] [[PubMed](#)]
27. Hou, L.; Kong, X.; Wang, Y.; Chao, J.; Li, C.; Dong, C.; Wang, Y.; Shuang, S. An Anthraquinone-based Highly Selective Colorimetric and Fluorometric Sensor for Sequential Detection of Cu^{2+} and S^{2-} with Intracellular Application. *J. Mater. Chem. B* **2017**, *5*, 8957–8966. [[CrossRef](#)] [[PubMed](#)]
28. Roberts, E.A.; Schilsky, M.L. AASLD Practice Guidelines: Diagnosis and Treatment of Wilson Disease: An Update. *Hepatology* **2008**, *47*, 2089–2111. [[CrossRef](#)] [[PubMed](#)]
29. Pfeiffer, R.F. Wilson’s Disease. *Handb. Clin. Neurol.* **2011**, *100*, 681–709.
30. Brewer, G.J.; Dick, R.D.; Johnson, V.D.; Fink, J.K.; Kluin, K.J.; Daniels, S. Treatment of Wilson’s Disease with Zinc XVI. Treatment during the Pediatric Years. *J. Lab. Clin. Med.* **2001**, *137*, 191–198. [[CrossRef](#)]

Disclaimer/Publisher’s Note: The statements, opinions and data contained in all publications are solely those of the individual author(s) and contributor(s) and not of MDPI and/or the editor(s). MDPI and/or the editor(s) disclaim responsibility for any injury to people or property resulting from any ideas, methods, instructions or products referred to in the content.